The 2015 World Congress on
Advances in Structural Engineering and Mechanics (ASEM15)
Incheon, Korea, August 25-29, 2015

Simulations of Fluidelastic Forces and Fretting Wear in U-Bend Tube Bundles of Steam Generators: Effect of Tube-Support Conditions

Marwan Hassan[1)] and Atef Mohany[2)]

[1)] *University of Guelph, Guelph, Ontario, Canada*
[2)] *University of Ontario Institute of Technology Oshawa, Ontario, Canada*
[1)] *mahassan@uoguelph.ca*
[2)] *atef.mohany@uoit.ca*

ABSTRACT

The structural integrity of tube bundles represents a major concern when dealing with high risk industries, such as nuclear steam generators, where the rupture of a tube or tubes will lead to the undesired mixing of the primary and secondary fluids. Flow-induced vibration is one of the major concerns that could compromise the structural integrity.
The vibration is caused by fluid flow excitation. While there are several excitation mechanisms that could contribute to these vibrations, fluidelastic instability is generally regarded as the most severe. When this mechanism prevails, it could cause serious damage to tube arrays in a very short period of time. The tubes are therefore stiffened by means of supports to avoid these vibrations. To accommodate the thermal expansion of the tube, as well as to facilitate the installation of these tube bundles, clearances are allowed between the tubes and their supports. Progressive tube wear and chemical cleaning gradually increases the clearances between the tubes and their supports, which can lead to more frequent and severe tube/support impact and rubbing. These increased impacts can lead to tube damage due to fatigue and/or wear at the support locations. This paper presents simulations of a loosely supported multi-span u-tube subjected to turbulence and fluidelastic instability forces. The mathematical model for the loosely-supported tubes and the fluidelastic instability model is presented. The model is then utilized to simulate the nonlinear response of a U-bend tube with flat bar supports subjected to crossflow. The effect of the support clearance as well as the support offset are investigated. Special attention is given to the tube/support interaction parameters that affect wear, such as impact and normal work rate.

NOMENCLATURE

$A, \bar{A}, a$	Flow channel area: unsteady, steady state, perturbation
$[C]$	Damping matrix
C_r	Radial tube clearance
d	Tube diameter
F_{cn}	Normal contact force
F_{dmp}	Damping force
F_f	Fluidelastic force
F_{pre}	Preload force
F_{spr}	Spring force
F_{turb}	Turbulence excitation force
$[K]$	Stiffness matrix
$[M]$	Mass matrix
$P, \bar{P}, p$	Pressure: unsteady, steady state, perturbation
S_o, S_a, S_s	Flow channel inlet, attachment point, separation point
t, T	Time, non-dimensional time
U	Pitch flow velocity
$U, \bar{U}, u$	Flow velocity: unsteady, steady state, perturbation
w	Tube displacement
ϕ	Spectral bound of turbulence forces
ϕ_D	Spectral bound of turbulence forces in drag direction
ϕ_L	Spectral bound of turbulence forces in lift direction
ρ_f	Fluid density
τ	Time lag

INTRODUCTION

Flow-induced vibrations of heat-exchanger tubes is identified as one of the most significant safety issue in operating nuclear steam generators. These issues are manifested in the form of failures due to fatigue and fretting wear at the supports. These failures can be very expensive in the case of nuclear steam generators. Therefore, flow induced vibrations have been the subject of extensive research in the past five decades to understand the phenomenon and to establish guideline for safe operations of these devices. The vibrations are excited by several excitation mechanisms. Turbulence and fluidelastic instability are the two dominant mechanisms in most heat exchangers (Païdoussis 1983, Weaver and Fitzpatrick, 1988). Fluidelastic instability is considered to be the most destructive mechanism and is characterized by the evolution of of large amplitude oscillations when the flow velocity exceeds certain threshold. If the threshold is exceeded,

tubes fail catastrophically in a short period of time. Detailed description of this mechanism can be found in the work of Price (1995). In order to avoid such failures counter measures such as limiting the flow velocity and stiffening the tube structure are considered. Therefore, supports are installed to provide a stiffer tube configuration. Tube/support assemblies are usually loose-fitting to accommodate tube thermal expansion and to facilitate the manufacturing and the assemble process. However, the existence of these supports allows for impacting and sliding against the support to take place. This in turn results in fretting wear damage potential at the tube support locations. Preventing such failures can be avoided by careful design with proper selection of anti-vibration bars especially in the U-bend region. Nevertheless some situations may arise from worn or ill-positioned supports. This may result in a larger than usual tube/support gaps. In such a case the tube may be exposed to high levels of impact and sliding force due to both turbulence and fluid-elastic coupling forces induced by the cross-flow. Prediction of tube response under the conditions of loose supports and fluidelastic force are a very complex process due to the nonlinearity of both the tube boundary conditions (loose supports) and fluidelastic forces. Predicting such wear requires the temporal records of quantities such impact force and the tube response. The paper deals with such predictive analyses, and attempts to present a simulation for a full U-bend tube configuration. The work also presents a systemic assessment of the determination of the appropriate number of anti-vibrations bars in the U-Bend region.

MODELLING

A loosely supported tube which is subjected to turbulence and fluidelastic force is described by the following equation:

$$[M]\{\ddot{w}\} + [C]\{\dot{w}\} + [K]\{w\} = \{F_{turb}(t)\} \quad (1)$$

where $w(t)$ is the response of the tube, *M* is the total mass, *C* is the damping coefficient, *K* is the system stiffness, and F_{turb} is the turbulence excitation force. Matrices *M*, *C*, and *K* contain the contributions of the fluid flow and the contact at the support. Due to the loose supports, the system stiffness and damping are nonlinear. One simplification of the system involves splitting the working space into two regions (states) within which the system behaves linearly. Therefore, the nonlinearity will represent transition from one state to another. It is possible to separate the flow and contact contributions to the system matrices in the form of forces and moved to the right-hand side of the above equation as follows:

$$[M_s]\{\ddot{w}\} + [C_s]\{\dot{w}\} + [K_s]\{w\} = \left\{F_{turb}(t) + F_f(t) + F_{pre}(t)\right\} \quad (2)$$

The above equation K_s and C_s represent the structural components of the system while M_s contains both the structural, internal flow, and added masses. $F_f(t)$ and $F_{turb}(t)$ are the

fluidelastic forces and the turbulence excitation forces, respectively. In some cases the external forces also has an additional constant component (preload, $F_{pre}(t)$). In general the tube structure is discretized using the finite elements.

The mathematical treatments of the impact force range from discretizing both of the tube and each support using beam and plate elements and applying a generalized overlap and contact algorithm to a much efficient specialized algorithm utilizing localized tube deformation effect. The later method will be utilized here and was described in full details by Hassan et al. (2002). However, brief description is presented in this section. Loose supports can be modelled by a number of massless bars attached by an equivalent contact spring and damper (Fig. 1). Impact takes place when the normal displacement component at the support location exceeds the tube support gap. In such event a corrective force is estimated based on the overlap displacement and applied as an external force to the system. The normal contact force (F_{cn}) is given by:

$$F_{cn} = F_{spr} + F_{dmp} \quad \text{for} \quad \omega_n(t) > C_r \tag{3}$$

$$F_{cn} = 0 \quad \text{for} \quad \omega_n(t) < C_r \tag{4}$$

Where F_{spr} and F_{dmp} are the spring and damping forces while C_r is the radial clearance. During the tube support contact, friction arises if the tube is excited to move in the tangential direction to the support. Several models were developed to deal with the steam generators tube bundles friction. These models include the Velocity Limited Friction Model (VLFM), the Spring Damper Friction Model (SDFM), and the Force Balance Friction Model (FBFM). Detailed description and comparison of these models can be found in the work of Hassan and Rogers (2005). In the current work, the FBFM with velocity feedback algorithm was used.

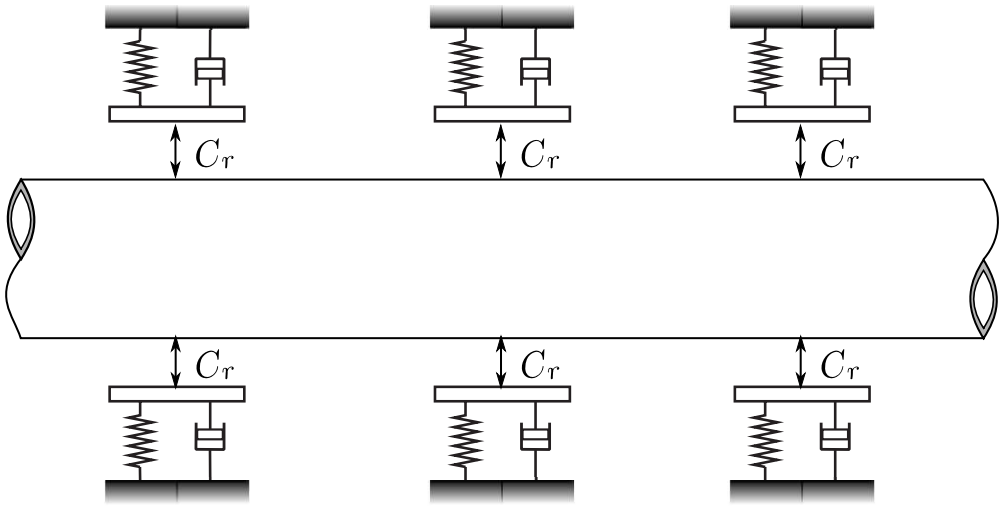

Figure 1: Tube-support model

As mentioned earlier turbulence excitation is a significant vibration mechanism that determines the long tem life of the tubes. Deep within the tube bundle, tubes are excited by the turbulence generated within the bundle which is governed by the tube bundle geometry. In general, fluid excitation due to turbulence is modelled as randomly distributed forces. The bounding power spectral density (PSD) measured by Oengören & Ziada (1998) for a tube array of pitch-to-diameter ratio (P/*d*) of 1.61 was utilized in this work to generate the time-domain fluid forces. Two force-time records are generated and applied in the lift and the drag directions and the turbulence forces are assumed to be fully correlated over the tube length. The power spectral density (PSD) of the dynamic force acting on any element *l* is expressed as:

$$S_{FF} = \frac{1}{4}\rho_f^2 d^3 U^3 l^2 \phi \quad (5)$$

where ρ_f, U, and ϕ are the fluid density, pitch flow velocity, and the spectral bound of the turbulence forces, respectively. For the triangular arrays with small spacing, the spectral bound for the lift ϕ_L and drag ϕ_D directions are given by:

$$\phi_L = 4.75 \times 10^{-3}\left(\frac{fd}{U}\right)^{-0.4} \quad for \quad \frac{fd}{U} < 0.43$$
$$\phi_L = 1.02 \times 10^{-4}\left(\frac{fd}{U}\right)^{-5} \quad for \quad \frac{fd}{U} > 0.43$$
$$\phi_D = 7.35 \times 10^{-4}\left(\frac{fd}{U}\right)^{-0.4} \quad for \quad \frac{fd}{U} < 0.53$$
$$\phi_D = 3.96 \times 10^{-5}\left(\frac{fd}{U}\right)^{-5} \quad for \quad \frac{fd}{U} > 0.53 \quad (6)$$

Fluidelastic instability forces are modeled using the time domain formulation introduced by Hassan et al. (2010, 2011). In this formulation, the complex flow through a tube array is approximated flow cells. Each flow cell consists of an active tube (flexible) attached to two flow channels and a number of boundary tubes (fixed), as shown in Fig. 2. The flow in each flow channel can be effectively modeled as a one-dimensional inviscid flow using a curvilinear coordinate *S*, which originates at the center of the active tube and extend to the flow cell inlet. The active tube affects the channel flow through the contact region from the attachment location (S_a) to the separation point (S_s). While the original formulation of the flow cell model (Lever and Weaver, 1982) assumes that the tube is vibrating at a steady-state amplitude at a frequency close to the natural frequency of the tube, the current model does not put such restriction and allows the tube to respond to both turbulence and FEI force. This is also very suitable for the case of loosely supported tubes which tend not to have a well-defined natural frequency which complicates the response prediction. The flow inside the channel is solved to predict the velocity and the pressure fields as a result

of deformation to the flow channels caused by the motion of the tube. The second replicates the boundary layer development as a result of the far field velocities and pressures determined in the flow channel subdomain. The solution algorithm involves decomposing the parameters of the flow channel (channel area A, flow velocity U, and pressure P) into first order terms ($\bar{A}$, $\overline{U}$, $\bar{P}$) and the second order terms (a, u, p) as follows:

$$A(s,t) = \bar{A}(s) + a(s,t) \quad (7)$$

$$U(s,t) = \overline{U}(s) + u(s,t) \quad (8)$$

$$P(s,t) = \bar{P}(s) + p(s,t) \quad (9)$$

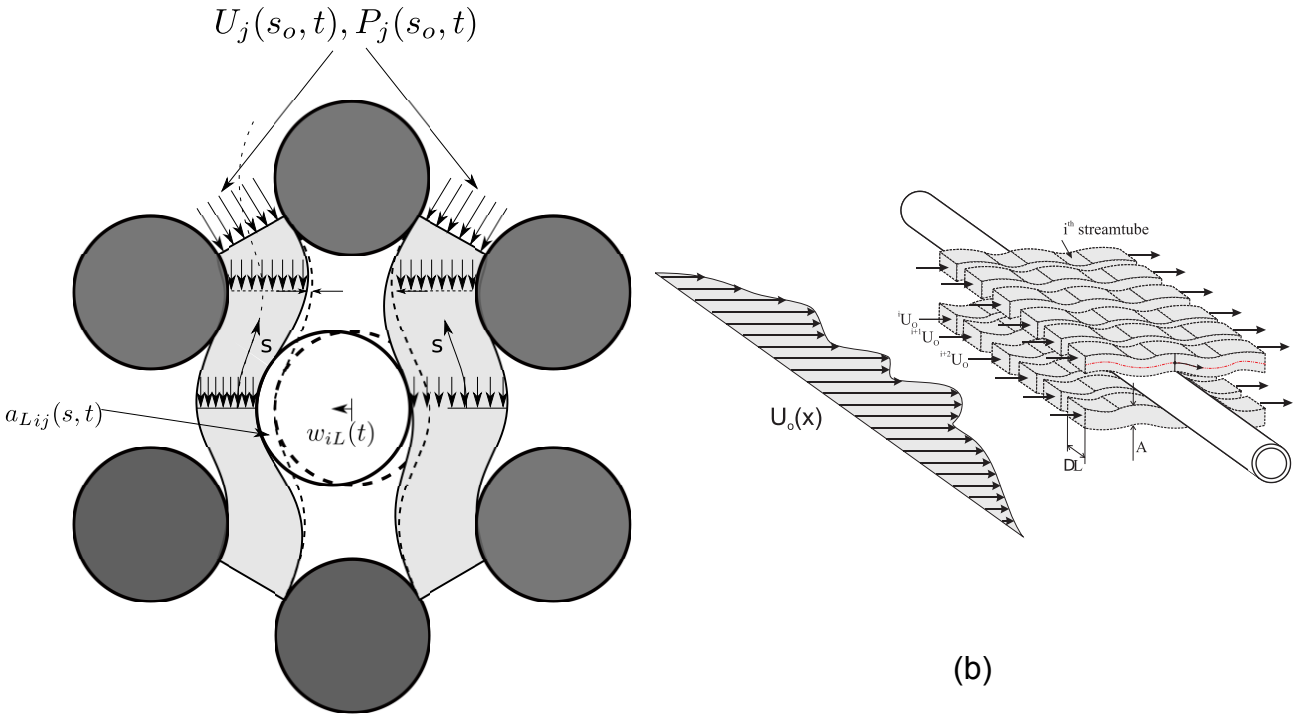

Figure 2: The flow cell model

The first order terms (steady) are related to the geometry of the flow channel while the second order terms (perturbations) are related to the motion of the flexible tube. The area perturbation can be directly calculated from the tube vibration time history as follows:

$$a(s,t) = w(t-\tau(s)) \cdot \hat{e}_t \cdot f(s) \tag{10}$$

τ is the time lag required for the flow to respond to the tube motion and can be attributed to the process of flow redistribution and momentum. This process is thought be caused by the flow inertia (Lever and Weaver, 1982), flow retardation (Price and Paidoussis, 1984), or vorticity convection and dissipation (Granger and Paidoussis, 1996). More discussion can be found in the work of El Bouzidi and Hassan (2015) regarding the time lag formulation. Now using the one dimensional continuity and momentum equations along the length of the flow channel, an expression describing the flow velocity and the pressure perturbations for a fluid of density ρ can be derived as follows:

$$u(s,t) = \frac{-1}{\bar{A}+a(s,t)}\left[U(-S_o)\cdot a(s,t) + \int_{-S_o}^{S} \frac{\partial a(s,t)}{\partial t} ds\right] \tag{11}$$

$$p(s,t) = P(-S_o) + \rho\left\{\frac{1}{2}U(-S_o)^2 - \frac{1}{2}U^2 - \int_{-S_o}^{S} \frac{\partial U}{\partial t} ds\right\} - \rho\left\{\frac{h}{2S_o}\cdot \int_{-S_o}^{S} U^2 ds\right\} \tag{12}$$

Inlet velocity $U(-S_o)$ and pressure $P(-S_o)$ are considered to be constant. Parameter h accounts for the resistance due to viscous losses. A reasonable estimate of the resistance coefficient can be obtained by assuming that it does not vary significantly with Reynolds number in the vicinity of the stability threshold for each array (Lever and Weaver (1986)). It was also shown that h does not greatly influence the stability threshold of the system. Therefore, an average value of 0.275 was used for all simulations. Additional effects such as the flow separation oscillation can be introduced which requires the modeling of the boundary at the tube/flow channel interface (Anderson et al. 2014).

SIMULATION PARAMETERS

Four different U-bend configurations were simulated. Each tube configuration was modeled by means of 91 three-dimensional beam elements, each of which has 12 DOF, as shown in Fig. 3a. The tube geometrical and material properties are listed in Table 1.

Table 1: Material and geometrical properties

Geometrical Properties	
Straight Leg Length	L=7 m
U-bend radius	1.9 m
Outside Diameter	d_o = 19 mm
Inside Diameter	d_i = 15.5 mm
Array	Parallel Triangle P/d=1.5
Material Properties	
Modulus of Elasticity	E=200 GPa
Density	ρ = 8304 kg/m^3
Poisson's Ratio	v = 0.28

Each tube is supported by 7 tube sheet supports (broached hole supports) in the hot and cold leg, as shown in Fig. 3b. The differences between these configurations lie in the number and locations of the flat bar supports. Typical flow distribution in the U-bend can be found in the work of Mohany et al. (2012). Such flow distribution was adopted in this work. Configurations 1, 2, 3, and 4 have 2, 4, 6, and 12 flat bar supports, respectively, as shown in Fig. 4. For each configuration, the clearance between the tube and the flat bar supports was varied between 0.1 mm to 1.0 mm. Each simulation was run for 10 sec with a time step of 0.01 msec. The rms streamwise and transverse responses of the tube were determined. In addition, the impact forces and the normal work rate were calculated.

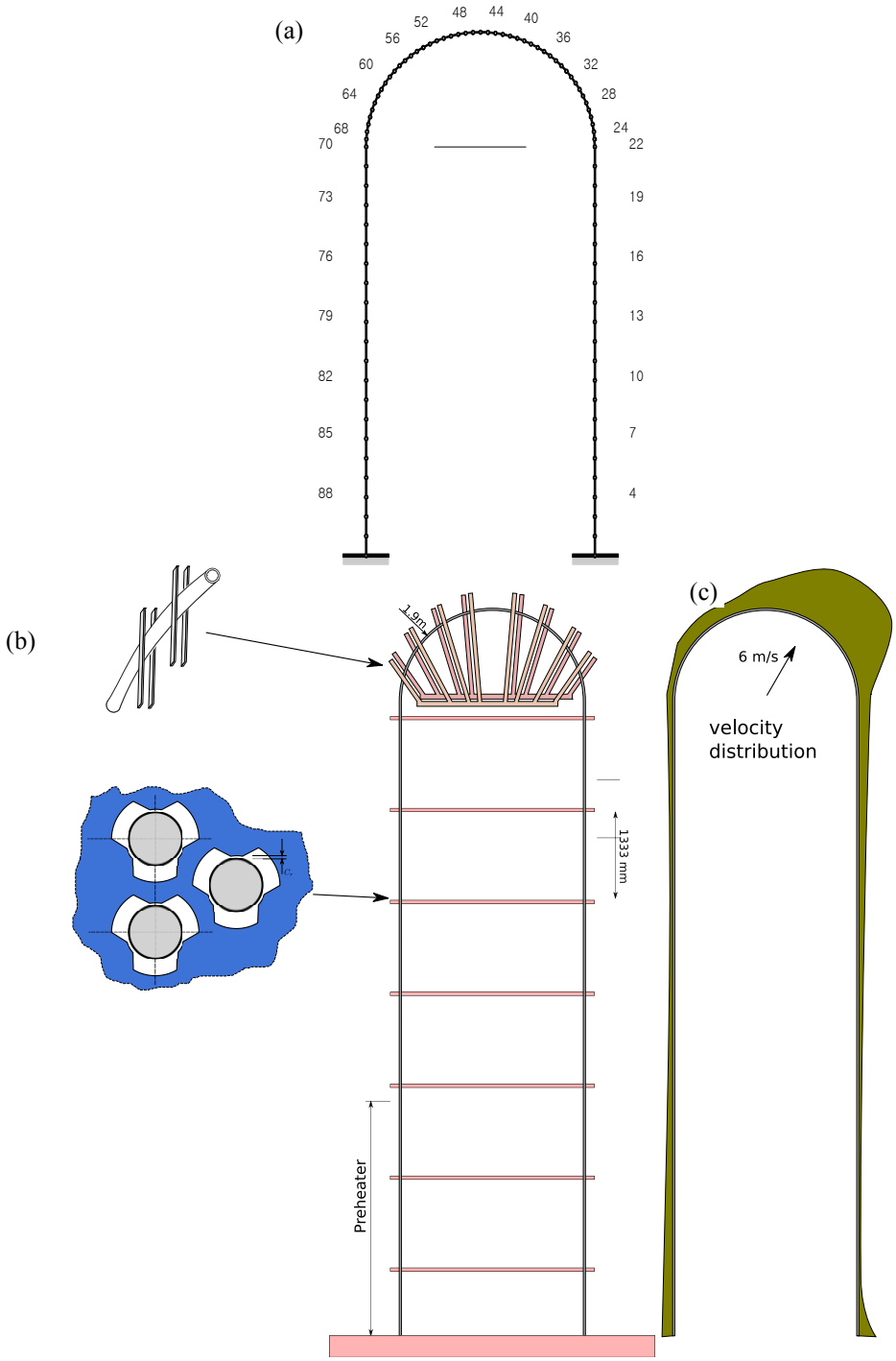

Figure 3: U-bend tube configuration showing: (a) FE nodes along the U-bend, (b) Tube broached hole and flat bar supports, as well as (c) The flow distribution in the U-bend region

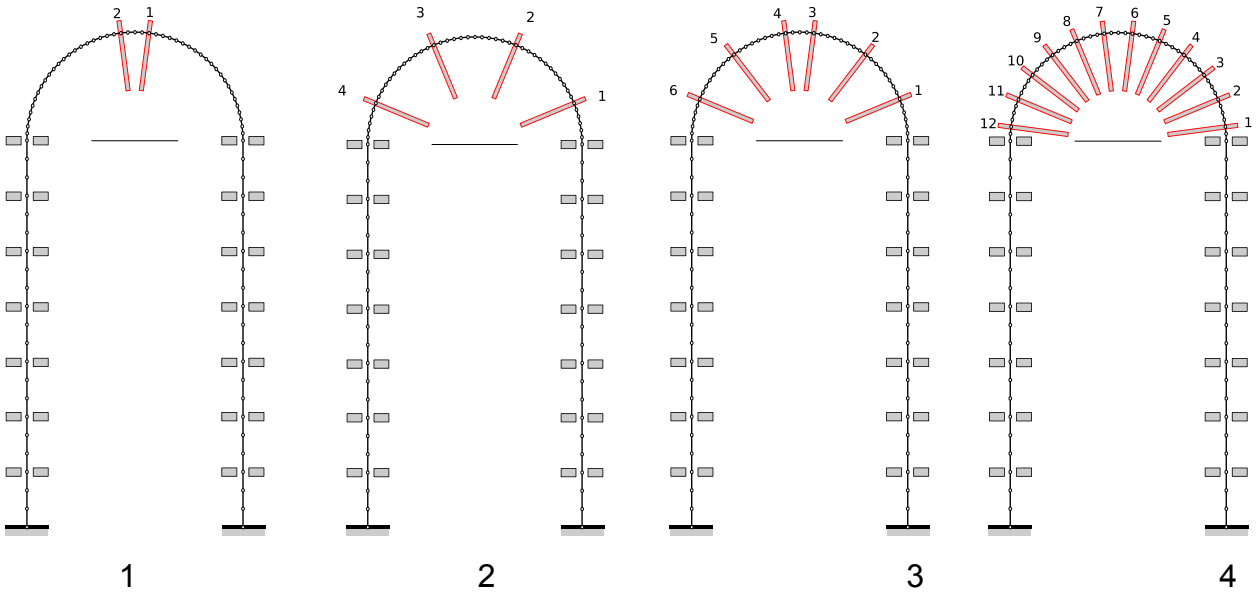

Figure 4: Tube support configurations with different number of flat bar supports

RESULTS

Figure 5 shows the rms tube response for the transverse and streamwise directions for Configurations 2, 3, and 4. Configuration 1 was found to be fluidelastically unstable resulting in very large tube response and an extremely high impact force levels. Therefore, the results of Configuration 1 was omitted from this section. The response shown in Figure 5 is for a clearance of 1.0 mm. The transverse response shows peaks at the mid-spans and valleys at the supports especially for the hot (nodes 1-20) and cold legs (nodes 60-91), refer to Fig. 3(a). For all configurations, the transverse response has its highest values in the U-bend region where the anti-vibrations bars are located. Configuration 2 exhibits the highest transverse response with values up to 6% of the tube diameter while the lowest response was found for Configuration 4. In addition, the response of Configuration 4 is almost flat in the U-bend region. This can be attributed to the large number of flat bars used. In general the streamwsie response is much smaller than the transverse response. However, configuration 4 shows a higher streamwise response than the transverse counterpart.

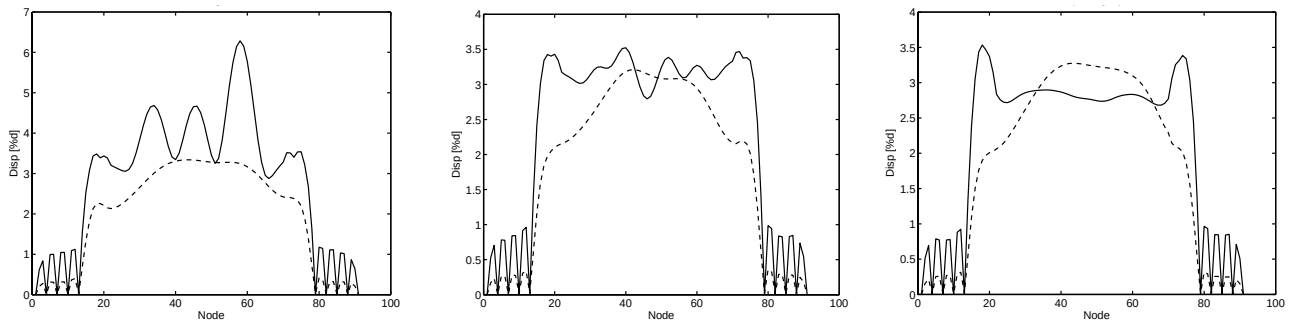

(a) (b) (c)

Figure 5: Streamwise (dotted line) and transverse (solid line) response along the tube nodes: (a) Configuration 2, (b) Configuration 3, (c) Configuration 4

Figure 6 shows the rms impact force at the U-bend anti-vibrations bars for two sets of support clearances (0.1 mm and 1.0 mm). The anti-vibrations bars were numbered 1, 2, 3, etc. starting from the hot side and counterclockwise towards the cold side (see Figure 4). For all configurations the impact force level is higher for larger support clearance. The highest level of impact force was found in configuration 2 (Fig. 5a). The higher the number of supports used the lower the impact force level. In addition, using more ant-vibration bars increases the ratio of the impact force level for the large and small clearances. Moreover, using more supports yields a better distribution of the impact force across the anti-vibration bars.

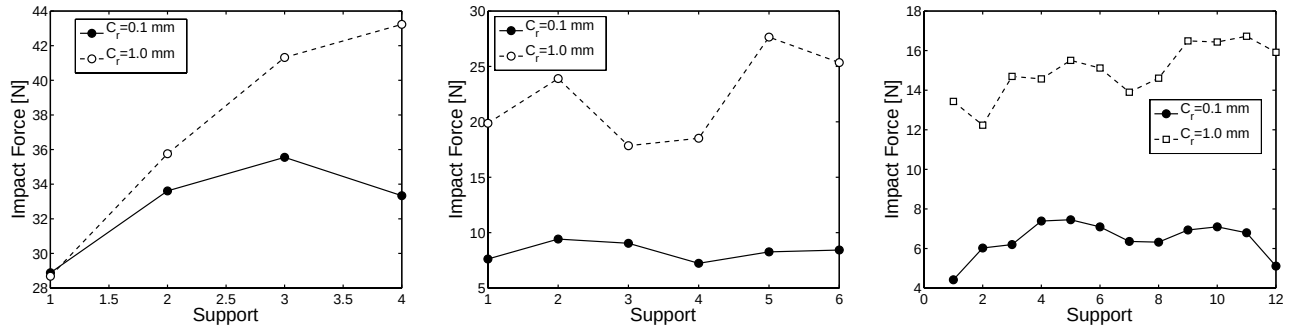

(a) (b) (c)

Figure 6: rms impact force at the supports located in the U-bend: (a) Configuration 2, (b) Configuration 3, (c) Configuration 4

Normal work is one of the most important parameters that is utilized to estimate the fretting wear potential. The normal work rate is defined as the normal component of contact force, F_{cn}, integrated over the sliding distance, w_s. As shown in Fig. 7, similar trends are manifested in the case of the impact force level and the normal work rate is lower as the number of supports is increased. For the clearance case of 1.0 mm, the predicted normal work rate of Configuration 2 is in the range of 45 to 70 mW. These considered extremely

high values as well-design steam generator are expected to have work rate levels in the range of a few mW. Configuration 3 also exhibits high values of work rate for a clearance of 1.0 mm. However, for the case of 0.1 mm the work rate is much lower (about 10 mW).

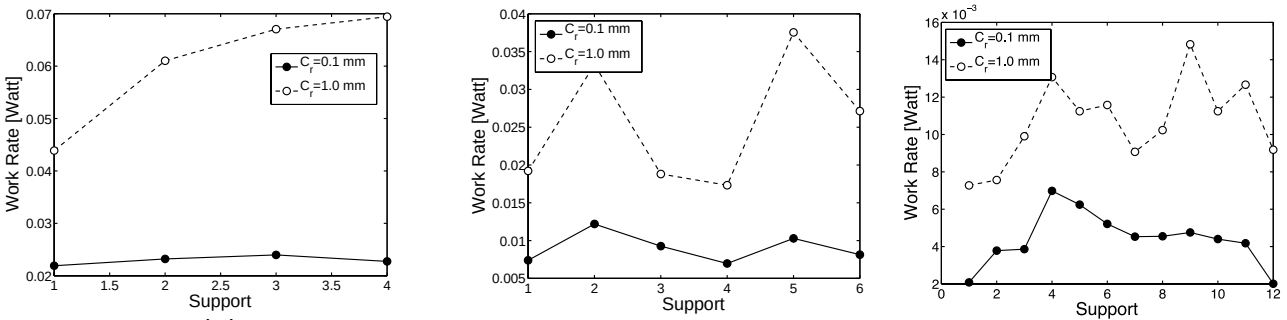

Figure 7: Normal work rate at the supports located in the U-bend: (a) Configuration 2, (b) Configuration 3, (c) Configuration 4

From the above the results, high and undesirable values of impact forces and normal work rates can be observed for lower number of anti-vibrations bars. With only 2-4 bars, Configurations 1 and 2 would not represent a viable design option. Configurations 3 and 4 with 6-12 bars seem to exhibit reasonable normal work rate values with configuration 3 being a borderline case. Since perfectly aligned support is more difficult to achieve as it requires tighter clearances and excellent manufacturing techniques, the more likely scenario is having supports with some form of offset between them. Therefore, in this work an attempt to investigate the effect of support offset is made. Configuration 3 will be utilized in this study as it has a marginal performance. Three offset cases were studied and are shown in Fig. 8. The offset scenarios are applied to the anti-vibration bars located in the U-bend region. Comparison in terms of value increase in the response, impact force, or normal work rate will always be in reference to the baseline case which is the zero offset.

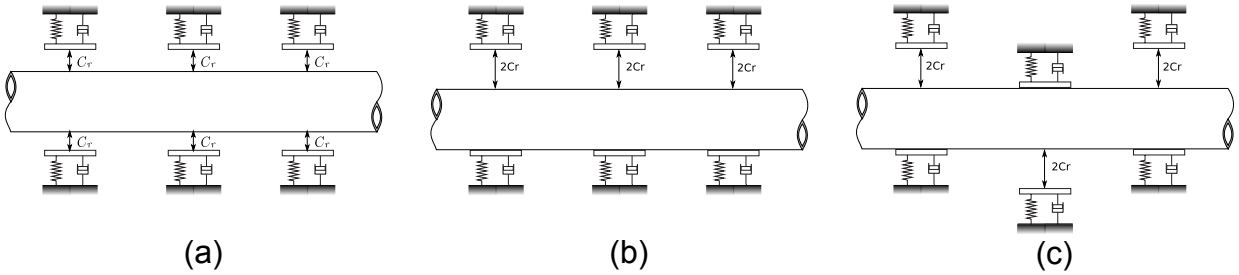

Figure 8: Tube support offset types: (a) zero offset, (b) one-side offset, (c) alternating offset

Figure 9 shows the tube response along the tube length for the three offset cases. The transverse response was greatly reduced for the alternate offset case. The reduction is particularly large in the neighborhood of the U-bend apex. Using the one-sided offset seems to increase the transverse response. Similarly, introducing the alternate support offset results in the largest reduction in the streamwise response. The greatest reduction is about 66% about the apex of the U-bend. However, about 20% increase in the tube response is obtained when using the one-sided offset.

The effect of the offset scenario on the rms impact forces is shown in Fig. 10. Results are shown for two clearance cases; small (0.1 mm) and large (1.0 mm). For the small clearance case (Fig. 10a), introducing the one-sided offset has little influence on the predicted impact force. However, the introduction of the alternate offset results in an increase in the impact force. The increase is the greatest at supports 3 and 4 which are close to the top of the U-bend. Introducing the one-sided offset results in a significant decrease in the impact force for the large clearance case. The reduction is in the range of 30% to 50% for supports 3-5. A significant increase in the impact force in the two middle supports (3 and 4) were predicted when the alternate offset was introduced. However the side supports (1, 2, 5, and 6) experiences smaller impact force levels.

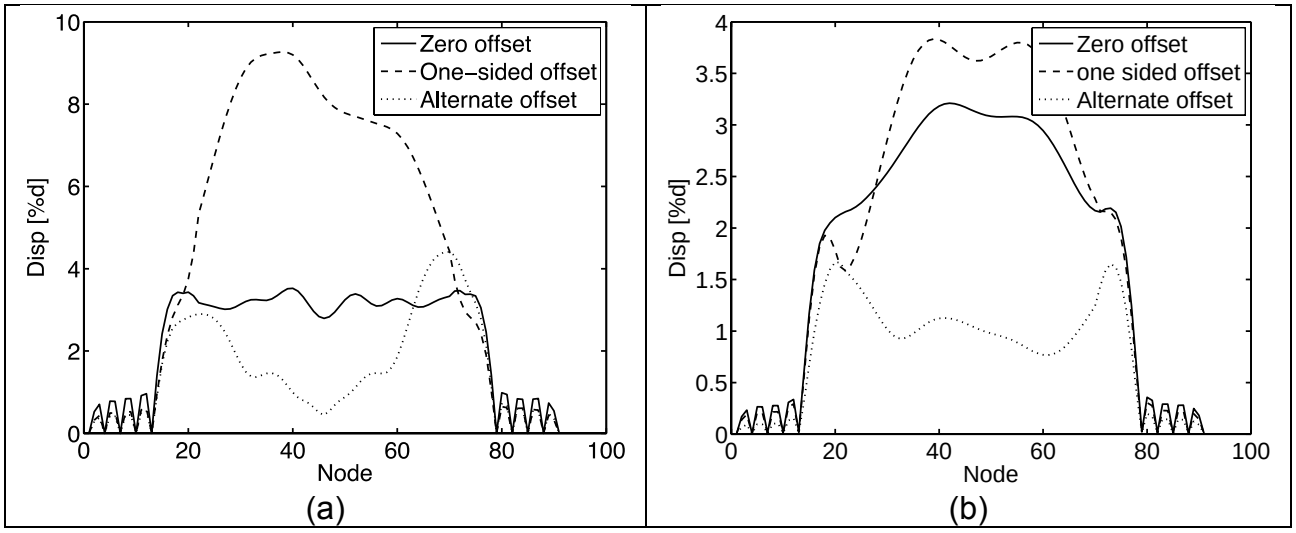

Figure 9: The effect of the support offset on the response along the tube nodes: (a) transverse, (b) streamwise

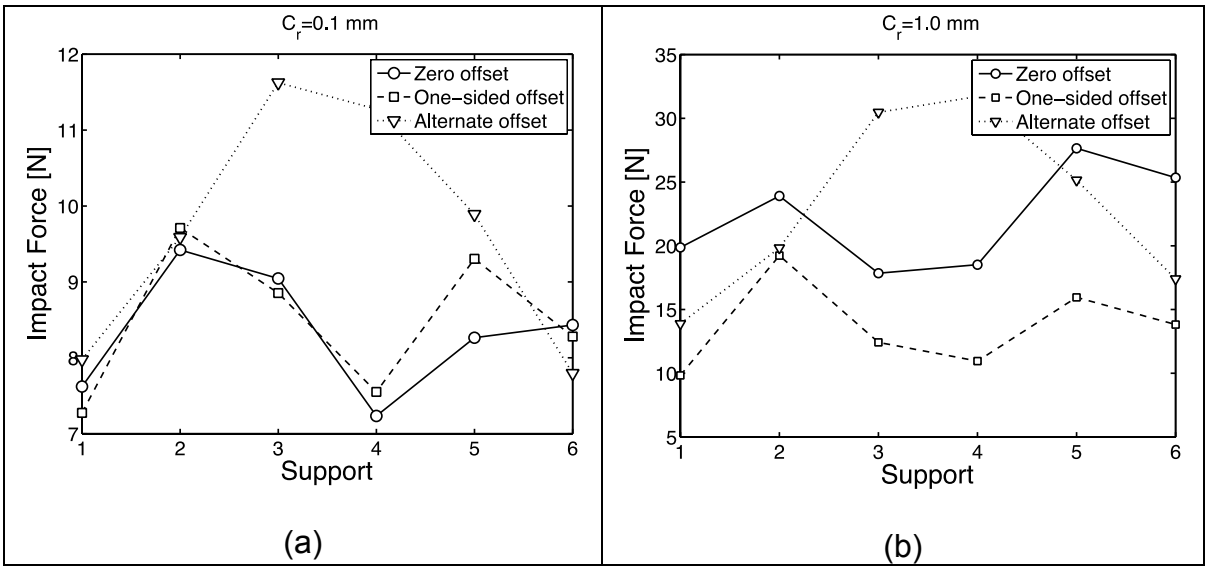

Figure 10: The effect of the support offset on the rms impact force: (a) 0.1 mm clearance, (b) 1.0 mm clearance

Normal work rate prediction for the two clearance cases is shown in Fig. 11. Small differences in the normal work rate level were predicted when introducing the one-sided offset for the small clearance. An increase in the normal work rate for supports 3 and 4 was observed for the alternate offset case (Fig. 11a). Introduction of the offset is shown to have an attenuating effect on the work rate for the large clearance.

The predicted response, impact force, and normal work rate shows the complexity of the dynamic system and its sensitivity to the conditions at the supports in terms of the clearance and the offset conditions. For example, the alternate offset conditions result in a relatively larger impact force at the top of the U-bend region which provides a larger contact force and a larger friction capacity. Increasing the friction capacity allows the means of energy dissipation. This large energy dissipation takes place at the top of the U-bend region, which provides the maximum moment arm and hence greater effectiveness. Conversely, the one-side offset results in less impact force level especially for the large clearance value (Fig. 10b). Smaller impact force levels limit the available friction capacity of the system. This in turn leads to a larger streamwise response (Fig. 9b). Hence, certain combinations of support clearance and offset conditions could promote larger streamwise oscillations and even could result in instability. This would explain some of the recent failures which took place in tube bundles in newly manufactured nuclear steam generators.

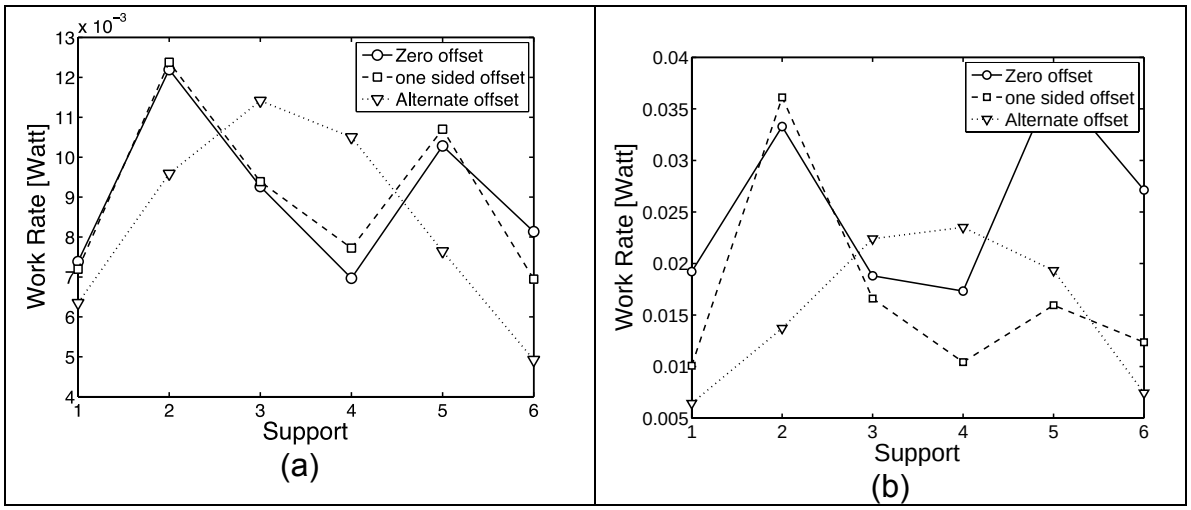

Figure 11: The effect of the support offset on the normal work rate: (a) 0.1 mm clearance, (b) 1.0 mm clearance

CONCLUSIONS

Simulations of a full scale U-Bend tube bundle were carried out. The simulations utilized modelling the structural dynamics of the tube including the effect of the loose supports. Modelling of the fluidelastic instability excitation was presented. Simulations were conducted for four configurations with 2, 4, 6, and 12 anti-vibrations bars installed in the U-bend region. For the rated flow velocity and density distribution used, Configuration 1 is unstable while Configuration 4 (with 12 supports) is stable with safe normal work rate levels. While using 4 anti-vibration bars seems to be stable, however, the normal work rates predicted are very high and such configuration can not be used. The third configuration was also stable with a relatively high normal work rates. Introducing the offset at the anti-vibrations bars seems to be beneficial in reducing the response, impact force and normal work rates, for large clearances. Little benefits can be gained from support offset if the clearance between the tube and its support is tight. In fact for small clearances such offset might results in higher tube response. The proposed model and the simulation results can be helpful in the design and prediction of flow-induced vibration of tube bundles in nuclear steam generators.

REFERENCES

Anderson, B., Hassan, M., Mohany, A., 2014. Modelling of fluidelastic instability in a square inline tube array including the boundary layer effect. Journal of Fluids and Structures 48, 362–375.

El Bouzidi, S., Hassan, M., (2015). An investigation of time lag causing fluidelastic instability in tube arrays. Journal of Fluids and Structures 57 (2015) 264–276.

Granger, S., and Païdoussis, M. P., 1996. An improvement to the quasi-steady model with application to cross-flow-induced vibration of tube array. Journal of Fluid Mech., 320, pp. 163–184.

Hassan, M., and Mohany, A., 2013. Fluidelastic instability modelling of loosely supported multi-span u-tubes in nuclear steam generators. ASME Journal of Pressure Vessel Technology, 135, p. 011306.

Hassan, M., and Rogers, R., 2005. Friction modelling of preloaded tube contact dynamics. Nuclear Engineering and Design, 235, pp. 2349–2357.

Hassan, M., Gerber, A., Omar, H., 2010. Numerical estimation of fluidelastic instability in tube arrays. ASME Journal of Pressure Vessel Technology 132 (4), 041307.

Hassan, M. A., Rogers, R. J., and Gerber, A. G., 2011. Damping-controlled fluidelastic instability forces in multi-span tubes with loose supports. Nuclear Engineering and Design, 241(8), pp. 2666–2673.

Lever, J. H., and Weaver, D. S., 1982. A theoretical model for the fluidelastic instability in heat exchanger tube bundles. ASME Journal of Pressure Vessel Technology, 104, pp. 104–147.

Lever, J., and Weaver, D., 1986. On the stability of heat exchanger tube bundles, part ii: Numerical results and comparison with experiments. Journal of Sound and Vibration, 107(3), pp. 393–410

Mohany, A., Janzen, V., Feenstra, P., and King, S., 2012. Experimental and numerical characterization of flow-induced vibration of multi-span U-tubes," ASME Journal of Pressure Vessel Technology, 134, p. 011301.

Oengören, A., and Ziada, S., 1998. An in-depth study of vortex shedding, acoustic resonance and turbulent forces in normal triangle tube arrays. Journal of Fluids and Structures, 12, pp. 717—758.

Price, S. J., 1995. A review of theoretical models for fluidelastic instability of cylinder arrays in cross-flow. Journal of Fluids and Structures, 9, pp. 463–518.

Païdoussis, M., 1983. A review of flow-induced vibrations in reactors and reactor components. Nuclear Engineering and Design, 74(1), pp. 31–60.

Weaver, D., and Fitzpatrick, J., 1988. A review of crossflow induced vibrations in heat exchanger tube arrays". Journal of Fluids and Structures, 2, pp. 73–93.